

High-resolution SPH simulations of merging white dwarfs

Pablo Lorén-Aguilar^{*1,2}, Alba G. Pedemonte^{1,2}, Jordi Isern^{3,2} and Enrique García-Berro^{1,2}

1

*Departament de Física Aplicada,
Escola Politècnica Superior de Castelldefels,
Universitat Politècnica de Catalunya
Avda. del Canal Olímpic s/n
08860 Castelldefels, Spain*

2

*Institute for Space Studies of Catalonia
c/ Gran Capità 2-4, Edif. Nexus 104
08034 Barcelona, Spain*

3

*Institut de Ciències de l'Espai (CSIC)
Facultat de Ciències, Campus UAB
08193 Bellaterra, Spain*

*E-mail: loren@fa.upc.edu, alba@fa.upc.edu, garcia@fa.upc.edu
isern@ieec.fcr.es*

We present the results of a series of high-resolution Smoothed Particle Hydrodynamics (SPH) simulations of merging white dwarfs. Our basic goals are to increase the resolution of the existing simulations in order to assess the reliability of the existing results, to explore a complete set of initial conditions and to study a wide enough range of masses of the coalescing white dwarfs. All this allows us to reach a complete picture of the merger process. We pay special attention to both the hydrodynamical and the chemical evolution. Furthermore we compute the pattern of gravitational wave emission of such systems and we assess whether or not LISA will be able to detect them.

*Supernovae: lights in the darkness (XXIII Trobades Científiques de la Mediterrània)
October 3-5 2007
Mao, Menorca, Spain*

*Speaker.

1. Introduction

Several interesting astrophysical phenomena have been invoked to be explained by the merger of two white dwarfs in a binary system. Among these phenomena perhaps the most exciting ones are that these mergers are probable progenitors of type Ia supernovae — see the recent review of Ref. [1] and references therein — likely progenitors of short gamma-ray bursts and magnetars in old populations [2] and possible progenitors of massive DAZ white dwarfs with dusty disks around them [3]. Moreover, they are guaranteed sources of gravitational waves which will be eventually detectable by future space-borne observatories like LISA [4]. However, the existing simulations of the coalescence process have been performed with low spatial resolution [5]. There is only one recent set of simulations in which a large number of particles [6] has been used, but the range of masses (and chemical compositions of the coalescing white dwarfs) studied in this work was rather limited, and only regular carbon–oxygen white dwarfs were considered. Consequently, the results of these simulations need to be confirmed and the range of parameters studied also needs to be expanded to include a wide range of masses and compositions of the merging white dwarfs. This is, precisely, the aim of this work. Here we show the preliminary results of an effort to explore a broad range of mergers involving white dwarfs of different masses and chemical compositions using high spatial resolution. To this end we have computed the coalescence of three white dwarf binary systems. The first two systems involve helium and carbon–oxygen white dwarfs (the $0.3 + 0.5 M_{\odot}$ and $0.4 + 0.8 M_{\odot}$ systems) and in the third case presented here two otherwise typical $0.6 M_{\odot}$ white dwarfs are involved.

2. Input Physics and method of calculation

We have followed the hydrodynamic evolution of the binary system using a SPH code. Since SPH is a well known technique, we will only describe here the most important features of our code. The interested reader can find more details in Refs. [4] and [5], whereas a general introduction to the SPH method can be found in the excellent review of Ref. [7]. Our SPH code uses a prescription for the artificial viscosity based in Riemann–solvers [8] together with time dependent viscosity parameters. Additionally, to suppress artificial viscosity forces in pure shear flows we also use the viscosity switch of Ref. [9]. In this way that the dissipative terms are essentially absent in most parts of the fluid and are only used when they are really necessary to resolve a shock. Within this approach, the SPH equations for the momentum and energy conservation read respectively

$$\frac{d\vec{v}_i}{dt} = - \sum_j m_j \left(\frac{P_i}{\rho_i^2} + \frac{P_j}{\rho_j^2} - \alpha \frac{v_{ij}^{\text{sig}}}{\bar{\rho}_{ij}} \vec{v}_{ij} \cdot \hat{e}_{ij} \right) \vec{r}_{ij} F_{ij} \quad (2.1)$$

$$\frac{du_i}{dt} = \frac{P_i}{\rho_i^2} \sum_j m_j \vec{v}_{ij} \cdot \vec{r}_{ij} \bar{F}_{ij} - \sum_j m_j \frac{v_{ij}^{\text{sig}}}{\bar{\rho}_{ij}} \left(\frac{1}{2} \alpha (\vec{v}_{ij} \cdot \hat{e}_{ij})^2 - \beta (u_i - u_j) \right) |\vec{r}_{ij}| \bar{F}_{ij} \quad (2.2)$$

where $\bar{\rho}_{ij} = (\rho_i + \rho_j)/2$ and $\bar{F}_{ij} \equiv (F_i + F_j)/2$, where F is a positive definite function which depends only on $|\vec{r}|$ and on the smoothing kernel h , used to express gradient of the kernel $\vec{\nabla} W_{ij} = \bar{F}_{ij} \vec{r}_{ij}$. The signal velocity is taken as $v_{ij}^{\text{sig}} = c_i + c_j - 4\vec{v}_{ij} \cdot \hat{e}_{ij}$ and the rest of the symbols have their usual meaning.

However, we have found that it is sometimes advisable to use a different formulation of the equation of energy conservation. Accordingly, for each timestep we compute the variation of the internal energy using Eq. (2.2) and simultaneously calculate the variation of temperature using:

$$\frac{dT_i}{dt} = - \sum_{j=1}^N \frac{m_j}{(C_v)_j} \frac{T_j}{\rho_i \rho_j} \left[\left(\frac{\partial P}{\partial T} \right)_{\rho} \right]_j \vec{v}_{ij} \cdot \vec{\nabla}_i W(|\vec{r}_{ij}|, h) + q_{\text{visc}} \quad (2.3)$$

where q_{visc} includes the contribution of viscous dissipation, which is computed in a way analogous to that of Eq. (2.2). For regions in which the temperatures are lower than 6×10^8 K or the densities are smaller than 6×10^3 g/cm³ Eq. (2.2) is adopted, whereas Eq. (2.3) is used in the rest of the fluid. Using this prescription we find that energy is conserved best.

We use a standard polynomic kernel [10], 3×10^5 SPH particles and the gravitational forces are evaluated using an octree [11]. Regarding the integration method we use a predictor–corrector numerical scheme with variable time step [12], which turns out to be quite accurate. Each particle is followed with individual time steps. With this procedure the energy and angular momentum of the system are conserved to a good accuracy. The equation of state adopted for this work is the sum of three components. Ions are treated as an ideal gas but taking into account Coulomb corrections. We have also incorporated the pressure of photons, which turns out to be important only when nuclear reactions become relevant. Finally the most important contribution is the pressure of degenerate electrons which is treated integrating the Fermi integrals. The nuclear network adopted here [13] incorporates 14 nuclei: He, C, O, Ne, Mg, Si, S, Ar, Ca, Ti, Cr, Fe, Ni and Zn. The reactions considered are captures of α particles, and the associated back reactions, the fussion of two C nuclei, and the reaction between C and O nuclei. All the rates are taken from Ref. [14]. The nuclear energy release is computed independently of the dynamical evolution with much smaller time-steps, assuming that the dynamical variables do not change much during these time-steps. Furthermore the energy loss by neutrino emission [15] is also computed.

3. Hydrodynamical and chemical evolution

All the simulations were performed following the same procedure. We relaxed the merging white dwarfs following closely the procedure previously adopted in Ref. [5], in which an artificial momentum loss was added to mimic the loss of energy due to the emission of gravitational waves during the inspiralling phase. Within this approach all the SPH particles describe almost keplerian orbits. This is illustrated in the top left panel of Fig. 1, which shows the temporal evolution of the SPH particles for the simulation of the coalescence of the $0.3 + 0.5 M_{\odot}$ double dwarf binary system. Soon after, the less massive white dwarf fills its Roche lobe and mass transfer begins, as can be seen in top central panel of Fig. 1. The top right panel of Fig. 1 shows that, after some time, the matter outflowing the secondary hits the surface of the primary white dwarf and spreads on top of it. Note as well that since the radius of white dwarfs scales as $M^{-1/3}$, as the secondary loses mass its radius increases and, hence, the mass–loss rate of the secondary increases, thus leading to a positive feedback of the process. As a consequence of this positive feedback an accretion arm is formed which extends from the remnant of the secondary white dwarf (central panels in Fig. 1) to the surface of the primary, more massive, white dwarf. This accretion arm becomes

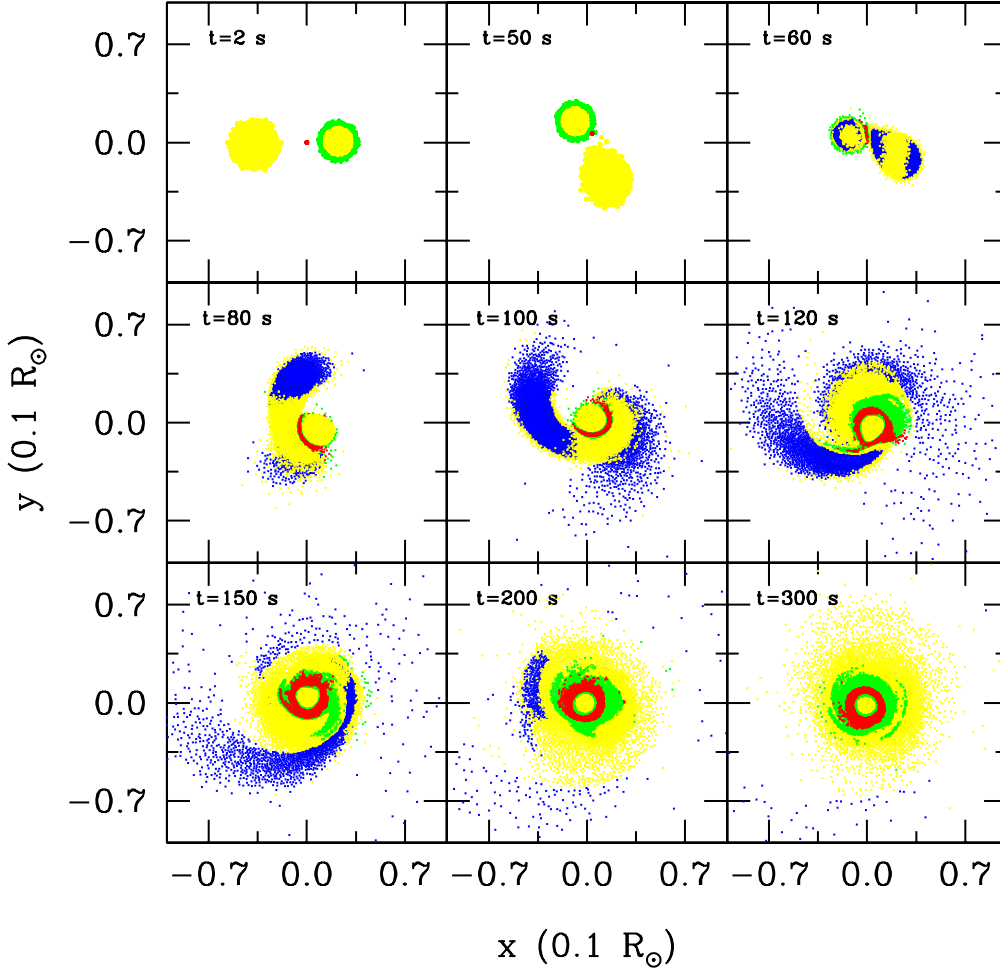


Figure 1: Temporal evolution of the positions of the SPH particles for the merging of the $0.3 + 0.5M_{\odot}$ double dwarf binary system. The positions of the SPH particles have been projected on the orbital plane. Time is shown — in seconds — on top of each panel. The colors indicate the different temperatures. See text for details.

entangled as a consequence of the orbital motion of the coalescing white dwarfs and adopts a spiral shape. Ultimately, the secondary is totally disrupted and a heavy disk is formed around the primary (bottom panels of Fig. 1). Note that final configuration has cylindrical symmetry, that all the orbits of the SPH particles belonging to the secondary have been circularized and that the spiral pattern has totally disappeared.

In Fig. 1 we have plotted the SPH particles using different colors to show the temperatures achieved during the coalescence process. Particles with temperatures smaller than 10^7 K are shown in yellow. Regions of the fluid with temperatures ranging from 10^7 K to 5×10^7 K are depicted in blue, whereas for particles with temperatures between 5×10^7 K and 10^8 K we have used green. Finally, particles with temperatures higher than 10^8 K are plotted in red. As can be seen in Fig. 1 the initial configurations of the merging white dwarfs are practically isothermal and only the external region of the secondary white dwarf is hotter than its isothermal core — top left panel of Fig. 1. This is due to the effect of tidal interactions. As time passes the particles outflowing the

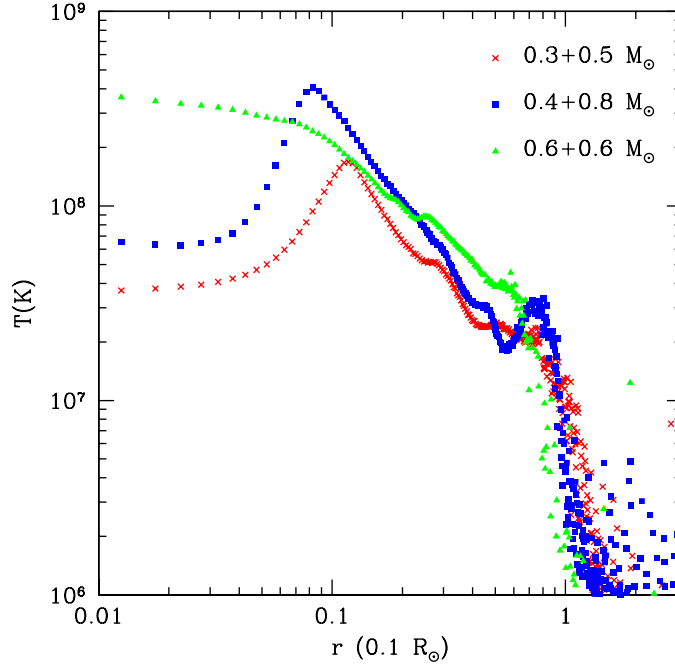


Figure 2: Radially averaged temperature profiles as a function of radius

secondary become accreted by the primary and a hotter spherical shell grows around the primary (top central panel). Note as well the presence of a hot spot at the location in which the previously discussed accretion stream collides with the surface of the primary. In the top right panel of Fig. 1 it can be seen how the secondary is already heavily deformed as a consequence of the ongoing process of disruption and how viscous dissipation due to tides heats its most deformed regions. It also can be appreciated how, simultaneously, the recently formed hot spot adopts a bar-like shape, which ultimately becomes more extended on top of the surface of the primary. Note as well that in the central panels of Fig. 1 it is quite apparent that some of the material colliding with the surface of the primary is bounced back. It can also be seen how the hot spot begins to extend over the surface of the primary (medium central panel) and how finally forms a corona around the primary (right central panel). In turn the spiral pattern of the accretion stream is quite apparent, but its temperature remains rather low ($\leq 5 \times 10^7$ K). Finally, in the bottom panels of Fig. 1 it can be seen that by the end of the simulations the accretion disk is rather cool and has an almost perfect cylindrical symmetry and a shallow gradient of temperatures whereas the region of maximum temperatures has an ellipsoidal shape surrounding the original surface of the primary and has a steep gradient of temperatures.

In Fig. 2 we show the temperature profiles at the end of the simulations for the three mergers studied here. We have averaged the temperatures of those particles close to the orbital plane. The average was done using cylindrical shells and the size of these shells was chosen in such a way that each of them contained a significant number of particles. As can be seen, for the $0.3 + 0.5 M_{\odot}$ and the $0.4 + 0.8 M_{\odot}$ systems, the region of maximum temperatures occurs off-center, at the edge of the original primary, in the region of accreted and shocked material, whereas for the merger in which two equal-mass $0.6 M_{\odot}$ white dwarfs coalesce the maximum temperature occurs at the center of the merged object, as it should be expected. In fact, the temperature profiles shown in this figure

Run	M_{WD}	M_{disk}	M_{acc}	M_{ej}	$T_{\text{max}} (\times 10^8) \text{ K}$	$R_{\text{disk}} (\times 0.1 R_{\odot})$
0.3+0.5	0.62	0.18	0.12	10^{-3}	6.0	2.0
0.4+0.8	0.92	0.28	0.12	10^{-3}	6.5	2.0
0.6+0.6	1.10	0.10	0.50	10^{-3}	6.2	0.7

Table 1: Summary of hydrodynamical results.

clearly show that the cores of the primaries in the first two simulations remain almost intact and, hence, are rather cold. These cores, in turn, are surrounded by a hot envelope which corresponds to the shocked material coming from the disrupted secondary. Nuclear reactions are responsible for the observed heating of the accreted matter, initially triggered in the shocked regions. The case in which two $0.6 M_{\odot}$ white dwarfs coalesce is somewhat different. In this case there is not a hot envelope around central object and, instead, the central region of the compact object is formed by the cores of the merging white dwarfs. Most of the temperature increase in this case is due to viscous heating since nuclear reactions are negligible because the increase in temperature of the shocked material is not enough to ignite carbon.

We have shown that in all the cases studied so far a self-gravitating structure forms after a few orbital periods. The time necessary for its formation depends on the system being studied, and ranges from 200 to 500 seconds. This self-gravitating structure consists in all cases of a compact central object, surrounded by a keplerian disk of variable extension. In table 1 we summarize the most relevant parameters of the three mergers studied here. Columns two, three, four and five list, respectively, the mass of the central white dwarf obtained after the disruption of the secondary, the mass of the keplerian disk, the accreted and the ejected mass. All the masses are expressed in solar units. In column six we display the maximum temperature achieved during the coalescence, whereas in column seven the radius of the disk is shown. As can be seen, for the first two simulations the accreted mass is approximately the same. In all three cases the mass ejected from the system (those particles which acquire velocities larger than the escape velocity) is very small. The maximum temperatures are roughly the same in all three cases. We have found that these temperatures are somewhat smaller than those obtained in our previous simulations [5]. Finally, the radial extension of the disks is the same for the first two simulations and it is considerably smaller for our last case. This is a natural behavior since in this last case the central object is rather massive.

In Fig. 3 we show the main characteristics of the merged configurations. In the left panels of this figure the rotational velocity is shown as a function of the radius. As can be seen, the central objects rotate as a rigid solid in all three cases. This behavior was already found in Refs. [5] and [6], and it is a consequence of the conservation of angular momentum. On top of the primary white dwarf a rapidly rotation shell can be found for the cases in which the two coalescing white dwarfs have different masses. Finally, for sufficiently large radius a rotationally-supported disk is found. The exact location where the disk begins can be easily found by looking at the left panels of Fig. 3, where the keplerian velocity is also shown as a dashed line. The change in the slope of the profile of the rotational velocity clearly marks the outer edge of the compact inner object and the beginning of the disk. All the disks extend up to some solar radii, but in the external regions of the disk some excess of artificial viscosity spreads the disk structure and no clear structure is formed. This can be seen in the left panels of Fig. 3, but perhaps it is more clearly appreciated in the right

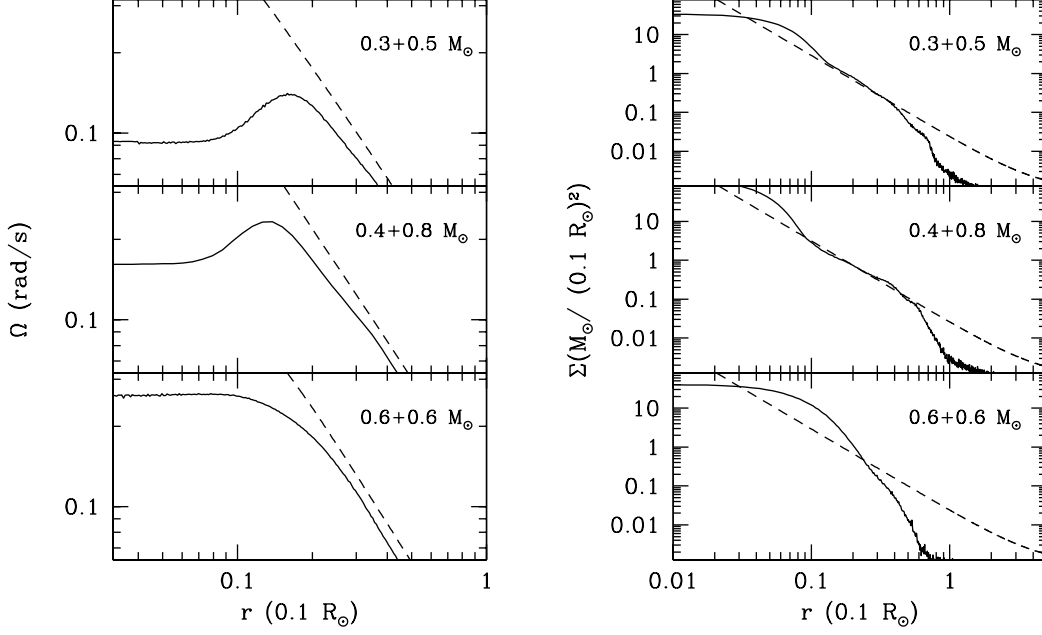


Figure 3: Left panels: rotational velocity of the merger products as a function of the radius. For the sake of comparison the keplerian velocity is also shown as a dashed line. Right panels: surface density profiles compared with the theoretical thin disk model profiles (dashed lines).

Run	0.3+0.5	0.4+0.8	0.6+0.6
He	0.94	0.95	0.0
C	2.5×10^{-2}	1.2×10^{-2}	0.4
O	3.7×10^{-2}	1.6×10^{-2}	0.6
Ca	6.0×10^{-5}	5.0×10^{-4}	0.0
Mg	2.0×10^{-9}	4.0×10^{-6}	0.0
S	3.0×10^{-7}	7.0×10^{-5}	0.0
Si	1.0×10^{-8}	3.0×10^{-5}	0.0
Fe	4.0×10^{-6}	2.0×10^{-5}	0.0

Table 2: Averaged chemical composition (by mass) of the heavy rotationally-supported disk obtained by the end of the coalescing process.

panels of this figure, where we have plotted the surface density as a function of the distance. For the sake of comparison the theoretical surface density of a thin disk analytical model [16] is also shown as a dashed line. As can be seen in this figure for the first two mergers there is a region where the analytical model and the numerical results are in good agreement. However, at large enough distances the SPH density profile falls off more rapidly than that of the theoretical model. This is due to the excess of artificial viscosity previously noted. In the case of the merger of two equal-mass $0.6M_\odot$ white dwarfs the agreement is poor. In this case, the symmetry of the system avoids the formation of a clear disk structure, giving rise instead to a rotating ellipsoid around the central compact object.

Finally, in Table 2 we show the chemical composition of the merged configurations. Note that for the cases in which a He white dwarf is involved, namely the $0.3 + 0.5M_\odot$ and the $0.4 + 0.8M_\odot$

binary systems, some matter is burnt, given that the temperatures achieved during the mergers is larger than 10^8 K. As a consequence we find non-negligible abundances of Ca, Mg, S, Si and Fe. Note as well that list the abundances in the rotationally-supported disks. The abundances of these elements are larger in the hot corona surrounding the central compact objects. This has important consequences because it is thought that some of the recently discovered metal-rich DA white dwarfs with dusty disks around them — also known as DAZd white dwarfs — could be formed by accretion of a minor planet. The origin of such minor planets still remains a mystery, since asteroids sufficiently close to the white dwarf would have not survived the AGB phase. However, planet formation in these metal-rich disks is expected to be rather efficient, thus providing a natural environment where minor planetary bodies could be formed and, ultimately, tidally disrupted to produce the observed abundance pattern in these white dwarfs [3].

4. Discussion

4.1 Gravitational Wave emission

We have also calculated the gravitational wave emission of the merging systems. In doing so we have used the slow-motion weak-field quadrupole approximation [17]

$$h_{jk}^{\text{TT}}(t, \vec{x}) = \frac{2G}{c^4 d} \frac{\partial^2 Q_{jk}^{\text{TT}}(t-R)}{\partial t^2} \quad (4.1)$$

where $t-R = t-d/c$ is the retarded time, d is the distance to the observer, and $Q_{jk}^{\text{TT}}(t-R)$ is the quadrupole momentum of the mass distribution, which is given by

$$\ddot{Q}_{jk}^{\text{TT}}(t-R) = \int \rho(\vec{x}, t-R) \left(x^j x^k - \frac{1}{3} x^2 \delta_{jk} \right) d^3x \quad (4.2)$$

To compute the quadrupole momentum of an ensemble of SPH particles, Eq. (4.2) has been discretized in the following way:

$$\ddot{Q}_{jk}^{\text{TT}}(t-R) \approx P_{ijkl}(\vec{N}) \sum_{p=1}^n m(p) [2v^k(p)v^l + x^k(p)a^l(p) + x^l(p)a^k(p)] \quad (4.3)$$

Where $m(p)$ is the mass of each SPH particle, and $x(p)$, $v(p)$ and $a(p)$ are, respectively, its position, velocity and acceleration and

$$P_{ijkl}(\vec{N}) \equiv (\delta_{ij} - N_i N_j)(\delta_{kl} - N_k N_l) - \frac{1}{2}(\delta_{ij} - N_i N_j)(\delta_{kl} - N_k N_l) \quad (4.4)$$

is the transverse-traceless projection operator onto the plane orthogonal to the outgoing wave direction, \vec{N} .

An example of our results is shown in figure 4, where the dimensionless strains h_+ and h_\times as a function of time for different inclinations are respectively shown for the $0.6 + 0.6 M_\odot$ merger studied here. As it can be seen in this figure, the emission of gravitational waves has initially an almost sinusoidal pattern of increasing frequency. Note that h_\times for $i = \pi/2$ is zero because the orbital plane is parallel to the line of sight. The different phases of the process, namely, spiralling, merger and ringdown, can be clearly distinguished. In any case it is clear that although during the first part

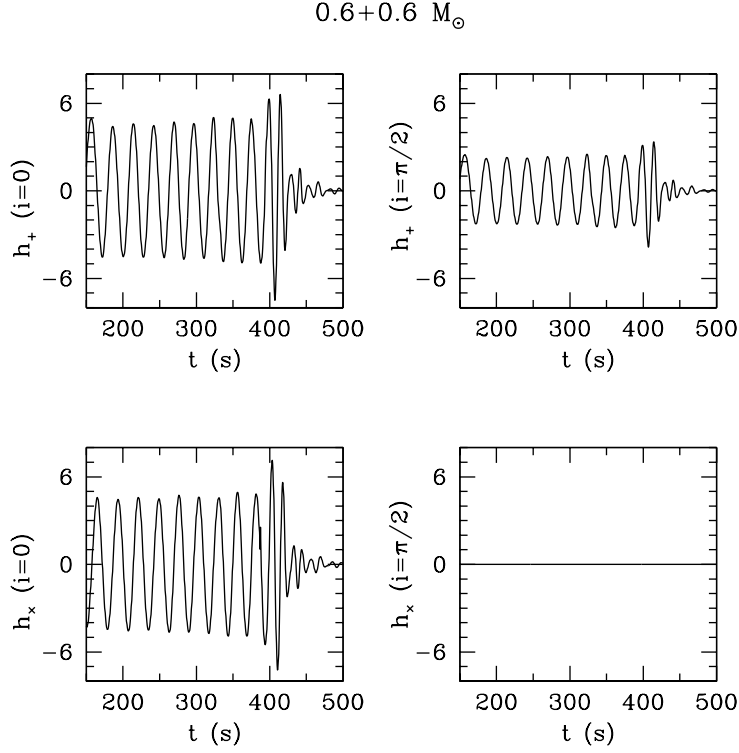


Figure 4: Gravitational wave emission from the coalescence of a $0.6 + 0.6 M_{\odot}$ binary. The dimensionless strains h_+ and h_{\times} are measured in units of 10^{-23} . The source is located at a distance of 10 kpc.

of simulation the same chirping pattern is found, once the merger proceeds the gravitational wave signal suddenly disappears on a short time scale, comparable to the orbital period.

In order to check whether or not LISA would be able to detect a close white dwarf binary system we have proceeded as follows. We have already shown that the most prominent feature of the emitted signal is its sudden disappearance in a couple of orbital periods and that the gravitational wave emission during the coalescence phase does not increase noticeably. Hence, the gravitational wave emission is dominated by the chirping phase. Hence, we have assumed that the orbital separation of the two white dwarfs is exactly that of our binary system *when mass transfer starts*. We have done so because, as explained before, we have added a small artificial acceleration term to the initial configuration in order to avoid an excessive computational demand at the very beginning of our simulations. This acceleration term is suppressed once the secondary begins to transfer mass onto the primary. Note, however, that the mass transfer starts when the secondary fills its Roche lobe and, consequently, this orbital separation is physically sound. We have further assumed that the integration time of LISA will be one year. We have checked that during this period the variation of the orbital separation is negligible. Of course, should the integration time be smaller the signal-to-noise ratio derived below would be smaller. Hence, our results should be regarded as an upper limit. The signal-to-noise ratio, η , is given by

$$\eta^2 = \int_{-\infty}^{+\infty} \frac{\tilde{h}^2(\omega)}{S(\omega)} \frac{d\omega}{2\pi} \quad (4.5)$$

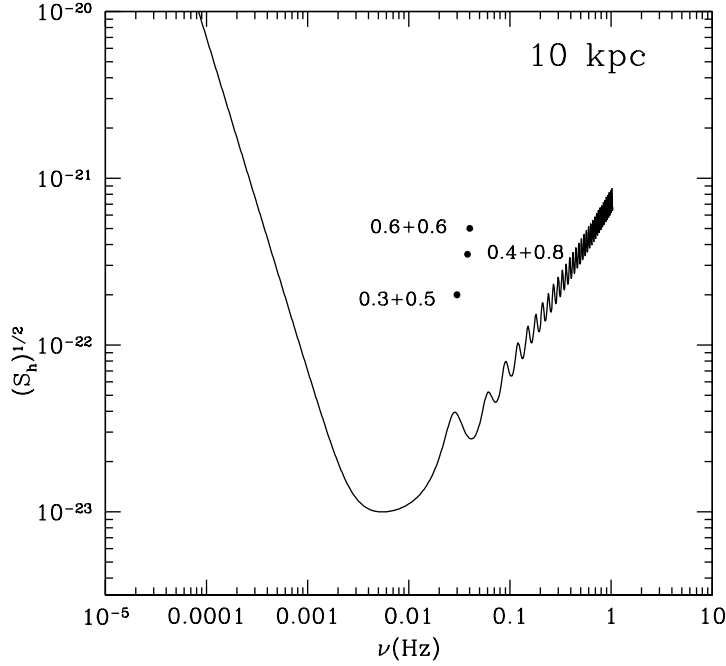


Figure 5: A comparison of the signal produced by the close white dwarf binary systems studied here, when a distance of 10 kpc is adopted, with the spectral distribution of noise of LISA for a one year integration period.

where $S(\omega) = S_h(\omega)\tau$ is the sensibility of LISA, τ is the integration period, and $\tilde{h}(\omega)$ is the Fourier Transform of the dimensionless strain. It can be easily shown that for a monochromatic gravitational wave $\eta = h(\omega)/S_h^{1/2}(\omega)$. The maximum distance, d_{\max} , at which LISA would be able to detect a close white dwarf binary system is then:

$$d_{\max} \approx 17 \left(\frac{5}{\eta} \right) \left(\frac{M}{M_{\odot}} \right)^{5/3} \left(\frac{\nu_0}{1 \text{ mHz}} \right)^{2/3} \left(\frac{10^{-23}}{\sqrt{S_h(\nu_0)}} \right) \text{ kpc} \quad (4.6)$$

where ν_0 is the frequency of gravitational wave, and M is the chirping mass.

$$M = \left(\mu M_{\text{tot}}^{2/3} \right)^{3/5} \quad (4.7)$$

being $\mu = m_1 m_2 / M_{\text{tot}}$ the reduced mass, and $M_{\text{tot}} = m_1 + m_2$ the total mass.

In order to evaluate the maximum distance at which LISA would be able to detect the close white dwarf binary systems studied here we have adopted $\eta = 5$. We have furthermore used the integrated sensibility of LISA¹.

In Fig. 5 we compare the signal produced by the close white dwarf binary systems studied in this paper, when a distance of 10 kpc is adopted, with the spectral distribution of noise of LISA for a one year integration period. As it can be seen, all of them will be eventually detected, at different signal-to-noise ratios.

¹<http://www.srl.caltech.edu/~shane/sensitivity>

Run	τ_{\min} (yr)	L (erg/s)	τ_{\max} (yr)	L (erg/s)
0.3+0.5	10^{11}	6×10^{29}	5×10^{-5}	10^{44}
0.4+0.8	10^{11}	5×10^{29}	9×10^{-4}	8×10^{43}
0.6+0.6	3×10^{11}	10^{29}	10^{-3}	4×10^{43}

Table 3: Typical viscous timescales

4.2 Long-term evolution

Despite the fact we have shown that no explosive nuclear burning takes place during the merging phase, this does not necessarily mean that such an explosion could not take place due to mass accretion from the disk at late times. If mass accretion occurs at rates smaller than $10^{-6} M_{\odot} \text{yr}^{-1}$ then, central carbon ignition is possible and SNIa is the most probable outcome. On the other hand, if the accretion rates are larger than this value, then off-center carbon ignition is the most probable outcome, giving rise to an inward propagating burning flame and an ONe white dwarf is likely to be formed [18, 20, 19] which might eventually become a neutron star by accretion-induced collapse [21, 22]. However, once the disk has been formed, the hydrodynamical time scale becomes dominant and does not allow to follow the subsequent disk evolution. However, some estimates of the accretion rate can still be done by considering the typical viscous transport timescales [23, 24, 25]

$$\tau_{\text{visc}} = \left(\frac{1}{T} \frac{dT}{dt} \right)^{-1} \quad (4.8)$$

where T is the rotational kinetic energy and

$$\frac{dT}{dt} = - \int \left(\frac{\partial \Omega}{\partial r} \right)^2 r^2 \eta(r) d^3 r \quad (4.9)$$

is its rate of change. In this expression Ω is the angular velocity, r is the radial cylindrical coordinate and η is the (physical) viscosity parameter, that depends on the viscous mechanism. If the disk is laminar and the viscosity is that of degenerate electrons then $\eta = 2.0 \times 10^{-5} \rho^{5/3} \text{g/cm s}$ [26, 27]. If, instead, the disk is turbulent the approximation $\eta = \rho v_t l_t / \text{Re}_c$ is valid [24]. In this equation l_t is the size of a turbulent cell — which we take to be the minimum of the radial and perpendicular scaleheights — $v_t \sim 0.1 c_s$ is the turbulent velocity and $\text{Re}_c \approx 5.0 \times 10^3$ is the critical Reynolds number. Using these prescriptions for the viscosities upper and lower limits to the typical transport timescales of the disk can be obtained. The total rotational kinetic energy dissipated L and the corresponding timescales using this approach are given in table 3. The associated accretion rates can be obtained taking into account that

$$L \sim \frac{M_{\text{acc}} v^2}{\tau} \sim \dot{M} v^2 \quad (4.10)$$

To compute the accretion rates we have adopted the keplerian velocity of the inner edge of the disk. For the case in which the laminar viscosity is used the resulting accretion rate turns out to be $10^{-20} M_{\odot} / \text{yr}$ rate, while in the case in which the turbulent viscosity is adopted we obtain that the accretion rate is $10^{-6} M_{\odot} / \text{yr}$ rate. Note that if the disk is turbulent, the accretion rate is close to the critical one, and an off-center ignition turns out to be a probable outcome. In order to check if

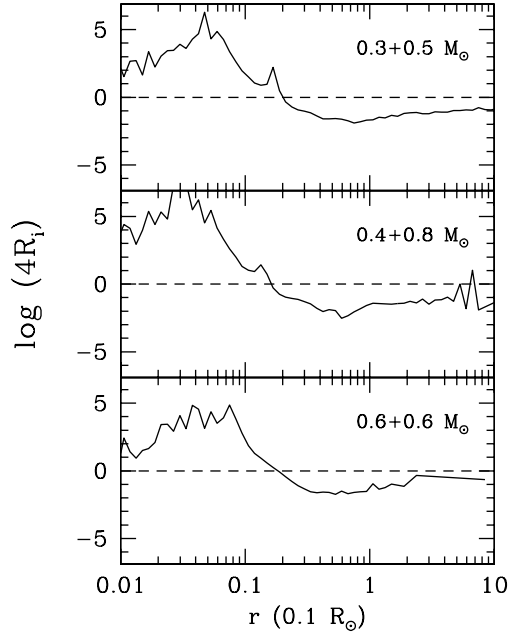


Figure 6: Richardson number

the disk is turbulent we have computed the Richardson number. If the Richardson number is larger than $1/4$ then, stability is guaranteed. If this is not the case the disk may still be turbulent, since this is only a necessary condition. In fig 6 we show the Richardson number as a function of the radial coordinate for the three cases studied here. As can be seen there the condition $Ri < 1/4$ is satisfied all over the disk. Hence, most likely the resulting disks are turbulent and, consequently, the result of the three mergers studied here will be the formation of an ONe white dwarf and, for large enough times, as the the disk is accreted accretion-induced collapse of the central compact object.

4.3 Short Gamma-Ray Bursts

Another interesting question is whether a binary system of white dwarfs could be considered as a possible engine for short gamma-ray bursts. Following a very simple model [28] we have calculated the accretion luminosity obtained from the interaction of high eccentricity stellar material with the recently formed disk. This model is intended to explain one of the most intriguing properties of gamma-ray bursts, namely the long-lasting X-ray emission after the main gamma-ray emission phase [29, 30, 31]. We have already shown that as a result of the merger of two white dwarfs of different masses, most of the SPH particles of the disrupted secondary form a keplerian disk. These SPH particles have circularized orbits. However, some material of the secondary is launched to highly eccentric orbits as well. This material will probably interact with the recently formed disk, releasing part of its kinetic energy in the form of electromagnetic waves. The time needed for a particle to be braked at a certain dissipation radius can be computed using the orbital radial equation

$$\frac{dr}{dt} = \pm \sqrt{\frac{2}{m} \left(E - V(r) - \frac{J^2}{2mr^2} \right)} \quad (4.11)$$

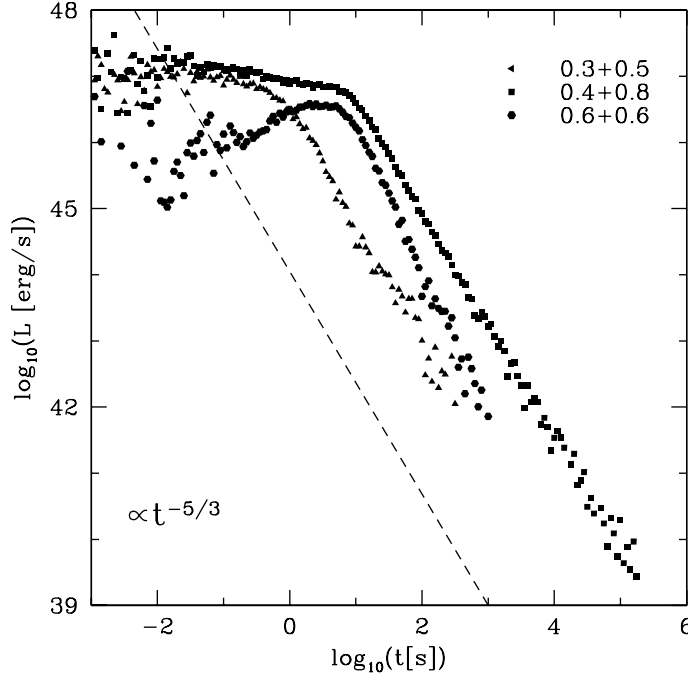


Figure 7: Expected fallback accretion luminosities for some of the most excentric particles of each simulation

After integration the result can be written as

$$\tau_{r_1, r_2} = \pm \int_{r_1}^{r_2} \frac{r dr}{\sqrt{Ar^2 + Br + C}}, \quad (4.12)$$

where $A = 2E/m$, $B = 2GM$ and $C = -(J/m)^2$. This integral can be solved analytically, and the solution turns out to be

$$\tau_{r_1, r_2} = \left[\frac{\sqrt{Ar^2 + Br + C}}{A} + \frac{B}{2A\sqrt{-A}} \arcsin\left(\frac{2Ar + B}{\sqrt{-D}}\right) \right]_{r_1}^{r_2} \quad (4.13)$$

where $D = 4AC - B^2$. Following closely Ref. [28] we have chosen the dissipation radius to be equal to the disk radius at the end of the simulation. In figure 7 it can be seen the accretion luminosity derived from our simulations. This luminosity has been computed assuming that these highly eccentric particles loose all its kinetic energy when interacting with the disk. Thus, the results shown in Fig. 7 can be regarded as an upper limit for the actual X-ray luminosity. Note that although the X-ray luminosities are smaller than those typically observed in short gamma-ray bursts — which are typically of $\sim 10^{49}$ erg/s — white dwarfs mergers predict the correct time dependence ($\propto t^{5/3}$) and, hence, cannot be totally discarded as possible sources of short gamma-ray bursts. However, an inspection of Fig. 7 reveals an important result. It is important to realize that although the $0.6 + 0.6M_{\odot}$ and the $0.3 + 0.5M_{\odot}$ models could in principle be candidates for some type of low-energy bursts, they cannot explain the long-term X-ray emission. Only the merger of two white dwarfs of masses 0.4 and $0.8M_{\odot}$ can, in principle, generate such a long-lasting emission, behavior that can be attributed to the higher degree of asymmetry of the system.

5. Conclusions

We have performed several high-resolution simulations of coalescing white dwarfs. In all cases, the merged configuration consists of a compact central object surrounded by a self-gravitating keplerian disk. For the $0.3 + 0.5 M_{\odot}$ and the $0.4 + 0.8 M_{\odot}$ cases the disk can be considered as a thin disk, whereas for the $0.6 + 0.6 M_{\odot}$ case we have found that the resulting disk resembles a rotating ellipsoid around the central object. We confirm the results obtained in previous works [5, 4, 6] and we find that only when one of the merging white dwarfs is a He white dwarf nuclear reactions are relevant. However none of the cases studied here show an explosive behaviour during the merging phase. Furthermore, no essential differences are found when the chemical abundances obtained here using an enhanced spatial resolution and a refined prescription for the artificial viscosity and those obtained in previous works [3] are compared. We have shown as well that the emission of gravitational waves from these kind of systems is strong enough to be observable by LISA. We have also shown these results also confirm previous findings and, thus, that they do not depend appreciably on the spatial resolution used to perform the calculations.

With respect to the long-term evolution of the mergers we have found that all our disks are potentially turbulent. This result implies that very large accretion rates from the disk onto the primary are expected. Despite our crude approximations, it is quite likely that these accretion rates would lead to an off-center carbon ignition and no supernova explosion is expected to occur in these systems, although an in depth study remains to be done. A detailed calculation of the evolution of the resulting disks, including an accurate description of the mechanisms of angular momentum transport, must therefore be done. Unfortunately this task is far beyond the current possibilities of SPH techniques. Finally, we have also found that white dwarf mergers might be possible candidates for the production of some low energy short gamma-ray bursts. The interaction of highly eccentric material with the disk might produce an accretion luminosity which reasonably fits the observed properties of these bursts.

Acknowledgments

This work has been partially supported by MEC grants AYA05-08013-C03-01 and 02, by the European Union FEDER funds and by the AGAUR.

References

- [1] Parthasarathy, M., Branch, D., Jeffery, D.J., & Baron, E., 2007, *New Astron. Rev.*, **51**, 524
- [2] Levan, A.J., Wynn, G.A., Chapman, R., Davies, M.B., King, A.R., Priddey, R.S., & Tanvir, N.R., 2006, *MNRAS*, **368**, L1
- [3] García-Berro, E., Lorén-Aguilar, P., Pedemonte, A.G., Isern, J., Bergeron, P., Dufour, P., & Brassard, P., 2007, *ApJ*, **661**, L179
- [4] Lorén-Aguilar, P., Guerrero, J., Isern, J., Lobo, J.A., & García-Berro, E., 2005, *MNRAS*, **356**, 627
- [5] Guerrero, J., García-Berro, E., & Isern, J., 2004, *A&A*, **413**, 257
- [6] Yoon, S.C., Podsiadlowski, P., & Rosswog, S., 2007, *MNRAS*, **380**, 933

- [7] Monaghan, J.J., 2005, *Rep. Prog. Phys.*, **68**, 1703
- [8] Monaghan, J.J., 1997, *J. Comp. Phys.*, **136**, 298
- [9] Balsara, D.S., 1995, *J. Comp. Phys.*, **121**, 357
- [10] Monaghan, J.J., & Lattanzio, J.C., 1985, *A&A*, **149**, 135
- [11] Barnes, J., & Hut, P., 1986, *Nature*, **324**, 446
- [12] Serna, A., Alimi, J.M., & Chièze, J.P., 1996, *ApJ*, **461**, 884
- [13] Benz, W., Hills, J.G., & Thielemann, F.K., 1989, *ApJ*, **342**, 986
- [14] Rauscher, T., & Thielemann, F.K., 2000, *Atom. Data & Nucl. Data Tables*, **75**, 1
- [15] Itoh, N., Nishikawa, A., & Kohyama, Y., 1996, *Apj*, **102**, 411
- [16] Livio, M., Pringle, J.E., & Wood, K., 2005, *ApJ*, **632**, L37
- [17] Misner, C.W., Thorne, K.S., & Wheeler, J.A., 1973, “*Gravitation*” (New York: W.H. Freeman)
- [18] Nomoto, K., & Iben, I., 1985, *ApJ*, **297**, 531
- [19] Ritossa, C., García-Berro, E., & Iben, I., 1999, *ApJ*, **515**, 381
- [20] García-Berro, E., & Iben, I., 1994, *ApJ*, 434, 306
- [21] Saio, H., & Nomoto, K., 1985, *A&A*, **150**, L21
- [22] Woosley, S.E & Weaver, T.A., 1986, *ARA&A*, **24**, 205
- [23] Mochkovitch, R. & Livio, M., 1989, *A&A*, **209**, 111
- [24] Mochkovitch, R. & Livio, M., 1990, *A&A*, **236**, 378
- [25] Ostriker, J.P. & Mark, J.W., 1968, *ApJ*, **151**, 1075
- [26] Durisen, R.H., 1973, *ApJ*, **183**, 205
- [27] Itoh, N., Kohyama, Y., & Takeuchi, H., 1987, *ApJ*, **317**, 733
- [28] Rosswog, S., 2007, *MNRAS*, **376**, L48
- [29] Burrows, D.N., Romano, P., Falcone, A., Kobayashi, S., Zhang, B., Moretti, A., O’Brien, P.T., Goad, M.R., Campana, S., Page, K.L., & 24 coauthors, 2005, *Science*, **309**, 1833
- [30] Nousek, J.A., Kouveliotou, C., Groupe, D., Page, K.L., Granot, J., Ramirez-Ruiz, E., Patel, S.K., Burrows, D.N., Mangano, V., Barthelmy, S., & 18 coauthors, 2006, *ApJ*, **642**, 389
- [31] O’Brien, P.T., Willingale, R., Osborne, J., Goad, M.R., Page, K.L., Vaughan, S., Rol, E., Beardmore, A., Godet, O., Hurkett, C.P., & 22 coauthors, 2006, *ApJ*, **647**, 1213